Soils and Foundations 2012;52(2):356–367

The Japanese Geotechnical Society

Soils and Foundations

www.sciencedirect.com
journal homepage: www.elsevier.com/locate/sandf

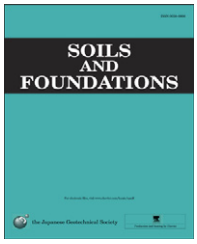

Dissipated energies and friction coefficients in granular flow by flume tests

Takaji Kokusho[a,*], Yuki Hiraga[b,1]

[a]*Civil & Environmental Engineering Department, Faculty of Science and Engineering, Chuo University, Japan*
[b]*Graduate School, Chuo University, Japan*

Available online 29 March 2012

Abstract

Laboratory flume tests on granular flow were conducted in order to investigate the influences of water content, grain size distribution, grain shape, fines content and flume angle on dissipated energy in the granular flow. Energy dissipated during the flow is evaluated from initial/residual potential energies and kinetic energy at the outlet of the flume. Though all parameters addressed here have measurable impact on the energy dissipation and the corresponding equivalent friction coefficient μ, it should be noted that the increase in fines content F_c up to a certain threshold tends to increase the equivalent friction coefficient μ. Beyond that threshold, the μ-value suddenly decreases due to a change in soil fabrics, transforming slow-speed granular flow to a high-speed mud flow. The evaluated μ-values for all tested cases have been found to be dependent on slope gradient.

Keywords: Granular flow; Flume test; Energy dissipation; Fines content; Friction coefficient

Introduction

Debris flows are natural disasters occurring with increasing frequency recently because of rapid urbanization in mountainous areas and also due to climate changes all over the world (Kokusho, 2005). Despite their frequent occurrence and devastation, the mechanism of debris flow has yet to be fully understood. Though debris flow is a high speed mass movement of granular materials mixed with water with a density 1.5–2.3 t/m^3 (Japanese Geotechnical Society, 2003), it has been studied in fluid mechanics more often than in solid or granular mechanics. In the laboratory, debris flow behavior was basically investigated by flume tests (e.g. Takahashi, 1980; Yasuda et al., 2008). Consequently, important geotechnical properties such as grain size distribution, grain shape, fines content have not been sufficiently considered in studying debris flow behavior.

In this laboratory test program, a series of flume tests have been performed on granular flows with special emphasis on the effect of geotechnical parameters. Energy dissipation and the corresponding equivalent friction coefficient in granular flow have been evaluated based on the energy balance in the flume test and compared among tests of different conditions to identify important parameters.

Test method and soil material

The flumes used in the tests for the energy calculation were 200 mm deep and 120 mm wide in inner cross-section and 3600 mm in length inclined with the angle θ as illustrated in Fig. 1. The upper 800 mm of the length was

*Corresponding author.
E-mail address: kokusho@civil.chuo-u.ac.jp (T. Kokusho).
[1]Now, Japan Railway East, Japan.

Peer review under responsibility of The Japanese Geotechnical Society
http://dx.doi.org/10.1016/j.sandf.2012.02.011

sectioned from the main part of the flume by a pneumatically driven gate, behind which granular soil mixed with water is placed just before the test. The slope angle θ of the flume was varied step by step from 20° to 30°. A dry soil mass of totally 10 kg, was slightly wetted first, placed behind the gate of the flume and added with a given quantity of water to make soil–water mixture of prescribed water content w_c. Once the granular flow starts by opening the gate, its discharge velocity v at the outlet of the flume was continuously measured by a digital image sensor as indicated in Fig. 2, together with the mass discharge M_D by an electronic balance as shown in Fig. 1.

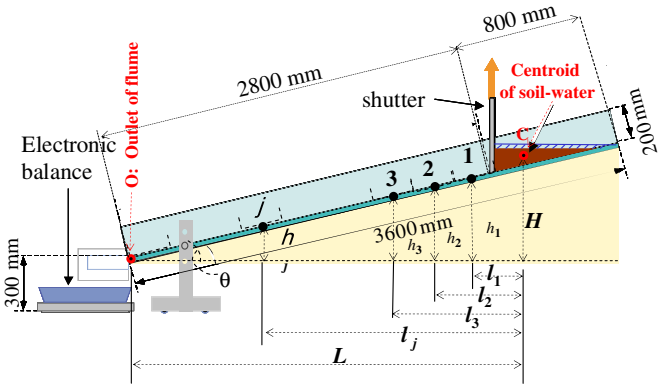

Fig. 1. Cross sectional sketch of test flume and its dimensions.

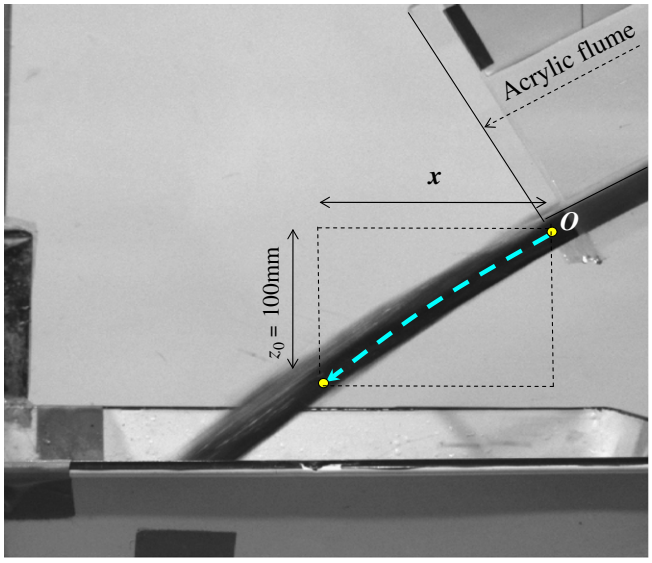

Fig. 2. Trajectory of flying soil particles of granular flow at the outlet of flume.

Soil materials used in the tests were fluvial sands/gravels of semi-round shapes of hard quality. Tested soil samples with parametrically varied mean grain size D_{50}, uniformity coefficient U_c and fines content F_c as well, were prepared in a different series of tests by appropriately mixing different sized particles. Rock flour from lime stone was used for non-plastic fines (particle size smaller than 0.075 mm) to be mixed with granular soils.

An acrylic flume was basically used for the tests, though a wooden flume was also used to examine the effect of the skin friction. Although it seems difficult to quantify the skin frictions exactly, a simple index test to evaluate their mutual differences was carried out, as illustrated in Fig. 3. Namely, a lump of dry soil (mean grain size $D_{50}=1.84$ mm shown later in Fig. 5), laterally constrained in a thin plastic film wall (400 g in weight, 10 cm square in the horizontal dimension), was placed on a slope so that it was in direct contact with the flume surface materials. Then the slope angle was raised slowly by a potable lift until the soil started to slide to determine the skin friction coefficients from the critical slope angle θ_{cr} as $\mu_{skin}=\tan\theta_{cr}$. The μ_{skin}-values thus obtained for the acrylic and wooden flumes were 0.43 and 0.50, respectively.

Energy balance considered in the test

The cumulative energy balance governing a granular flow in the flume test from the start to the end, is expressed as follows:

$$E_D = E_{PI} - E_K - E_{PR} \tag{1}$$

where E_D is the dissipated energy in granular flow, E_{PI} the initial potential energy, E_K the kinetic energy preserved at the flume end and E_{PR} the residual potential energy at the end of the test. Based on the measured values, the kinetic

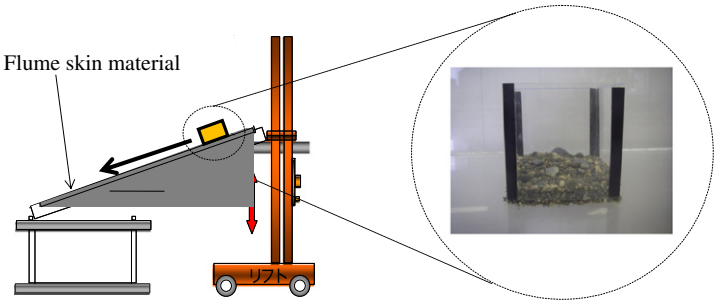

Fig. 3. Schematic illustration how to measure flume skin friction μ_{skin}.

energy at the outlet of the flume E_K can be calculated as

$$E_K = \sum_i m_D(i\Delta t)[v(i\Delta t)]^2/2 \tag{2}$$

where the mass discharge increment $m_D(i\Delta t)$ at ith time increment (Δt=a time increment), can be calculated from the mass discharge M_D as

$$m_D(i\Delta t) = M_D(i\Delta t) - M_D((i-1)\Delta t) \tag{3}$$

The flow velocity of grains at the outlet v may be evaluated from the trajectory, shown in Fig. 2, of flying grains, which is monitored by the digital image sensor. The basic equations used here are from Newtonian physics; $x = vt\cos\theta$ and $z = vt\sin\theta + (gt^2/2)$, for the horizontal and vertical distances from the outlet (Point O in Fig. 2) at a time t, respectively. By deleting t in these equations

$$z = x\sin\theta/\cos\theta + gx^2/(2v^2\cos^2\theta)$$

can be easily derived. Hence, the flow velocity of grains at the outlet $v(i\Delta t)$ at ith time increment in Eq. (2) is calculated as

$$v(i\Delta t) = \sqrt{\frac{g}{z_0(1+\cos 2\theta) - x(i\Delta t)\sin 2\theta}}\cdot x(i\Delta t) \tag{4}$$

here, g is the acceleration of gravity, $z=z_0$ the drop height from Point O (100 mm constant), $x(i\Delta t)$ the horizontal flying distance for grains corresponding to the vertical distance z_0 at ith time increment. The flow velocity measured in this way, though not yet calibrated by other methods, seems to be reliable because it is based only on the very simple kinematic equations and two test results from the same test condition generally show satisfactory repeatability as will be mentioned later.

The residual potential energy E_{PR} in Eq. (1) can be calculated by measuring residual soil mass in individual sections of the flume after the end of the test as

$$E_{PR} = g\sum_j m_R(j)\cdot h_j \tag{5}$$

where, $m_R(j)$ is the residual soil mass at jth interval (200 mm each) of the flume, and h_j the height at the center of each interval from the flume outlet O as indicated in Fig. 1. The initial potential energy is

$$E_{PI} = MgH \tag{6}$$

where H the height measured from the outlet of the flume, Point O, to the centroid of the soil–water mixture, Point C, initially charged behind the gate. The total mass of the soil–water mixture M can be expressed as

$$M = \sum_i m_D(i\Delta t) + \sum_j m_R(j) \tag{7}$$

Thus, the energy dissipated in the soil mass during a single batch test from the start to the end of a flow, E_D, was evaluated from Eq. (1) using Eqs. (2)–(7) as

$$E_D = gH\left[\sum_i m_D(i\Delta t) + \sum_j m_R(j)\right] - \sum_i m_D(i\Delta t)[v(i\Delta t)]^2/2 - g\sum_j m_R(j)\cdot h_j \tag{8}$$

The time increment Δt was chosen as 0.020–0.017 s in the measurement of $m_D(i\Delta t)$ and $v(i\Delta t)$ above.

It is easy to understand that the dissipated energy e_D for unit soil mass to flow in unit horizontal distance can be calculated from the energy loss E_D in Eq. (8) as

$$e_D = E_D \Big/ \left(L\sum_i m_D(i\Delta t) + \sum_j m_{r_j} l_j\right) \tag{9}$$

where, L the horizontal distance from the initial centroid (Point C) of soil–water mixture behind the gate to the flume outlet O, and l_j=horizontal distance from Point C to the center of the jth section of the flume. This value e_D may represent the average energy dissipated in a soil block of unit mass as illustrated in Fig. 4 to flow in a unit horizontal distance during a single flow test from start to end. Here, the units of length such as L, l_j and mass such as M_D, m_{r_j} are chosen as m and kg, respectively so that the unit of e_D is J/kg/m.

The potential energy change for the same soil mass flowing in the unit horizontal distance is $g\tan\theta$. Hence, the ratio of the dissipated energy in the granular flow to the corresponding potential energy denoted here as R_d is

$$R_d = e_D/(g\tan\theta) \tag{10}$$

The dissipated energy ratio R_d can serve as an index, such that the smaller the R_d-value, the longer the granular flow may travel. An equivalent friction coefficient $\mu=\tan\phi$ between the soil mass and the flume (ϕ=friction angle) is introduced, here. The value μ actually reflects energy loss not only by the flume skin friction but also by inter-particle movements. Then, the dissipated energy for a unit mass shown in Fig. 4 to flow in unit horizontal distance is

$$e_D = \mu g\cos\theta \times (1/\cos\theta) = \mu g$$

Hence from Eq. (10), the equivalent friction coefficient manifested on average during a single flow event is

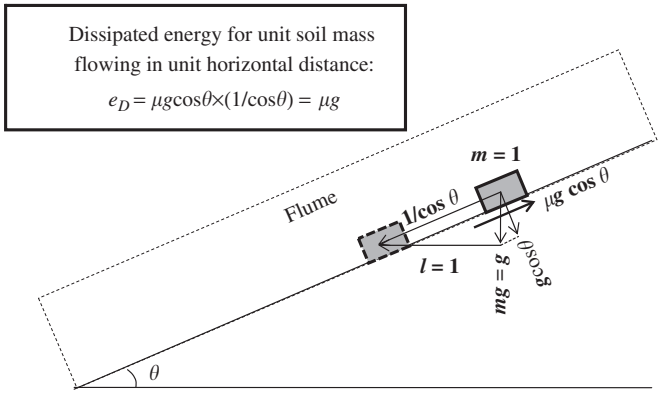

Fig. 4. Illustration of unit soil mass flowing in unit horizontal distance on the flume and its loss energy e_D.

Table 1
Test conditions and results for G-series (variable parameters: θ, w_c, D_{50}, U_c, flume skin friction, particle shape).

Test no.	Flume skin	θ (°)	Total mass (kg)	Water cont. (%)	D_{50} (mm)	U_c	U_c'	Grain shape R/C	M_D (kg)	M_R (kg)	Initial centr. height H (m)	Horiz. flow dist. L (m)	$\sum(l_j m_j)$ (kg m)	Initial potent. energy E_P (J)	Kinetic energy E_k (J)	Resid. potent. energy E_{PR} (J)	Dissip. energy E_D (J)	Dissip. energy e_D (J/m/kg)	$R_d=e_{DP}/(g\tan\theta)$	Friction coeff. $\mu=e_{DP}/g$	Max. dev. of μ divided by av. of μ
G-1	Acryl	30	15.0	50	14.43	4.25	1.03	R	14.85	0.15	1.58	2.58	0.08	232.3	82.8	1.9	147.6	3.85	0.680	0.392	0.012
G-2	Acryl	30	13.5	35	14.43	4.25	1.03	R	13.37	0.24	1.57	2.57	0.12	209.5	63.1	3.0	143.4	4.16	0.735	0.424	0.002
G-3	Acryl	30	15.0	50	5.77	4.22	0.94	R	14.84	0.16	1.58	2.58	0.12	232.2	78.6	1.8	151.9	3.95	0.699	0.404	0.023
G-4	Acryl	30	13.5	35	5.77	4.22	0.94	R	13.22	0.27	1.57	2.57	0.23	207.4	58.9	2.8	145.8	4.26	0.754	0.435	0.002
G-5	Acryl	30	15.0	50	1.84	4.26	1.01	R	14.54	0.46	1.58	2.58	0.56	232.3	62.4	3.8	166.1	4.36	0.771	0.445	0.000
G-6	Acryl	30	13.5	35	1.84	4.26	1.01	R	12.97	0.53	1.57	2.57	0.64	207.7	42.6	4.4	160.7	4.73	0.836	0.483	0.003
G-7	Acryl	26.5	15.0	50	14.43	4.25	1.03	R	15.03	0.76	1.43	2.68	0.65	221.2	61.9	7.0	152.4	3.72	0.762	0.380	0.002
G-8	Acryl	26.5	13.5	35	14.43	4.25	1.03	R	13.49	0.80	1.42	2.68	0.70	198.8	49.2	7.3	142.3	3.86	0.791	0.394	0.022
G-9	Acryl	26.5	15.0	50	5.77	4.22	0.94	R	14.76	0.32	1.43	2.68	0.28	211.3	60.7	2.8	147.8	3.71	0.759	0.378	0.028
G-10	Acryl	26.5	13.5	35	5.77	4.22	0.94	R	13.38	0.20	1.42	2.68	0.19	188.9	41.0	1.7	146.2	4.06	0.830	0.414	0.001
G-11	Acryl	26.5	15.0	50	1.84	4.26	1.01	R	14.00	1.01	1.43	2.68	1.26	210.2	42.4	7.2	160.6	4.14	0.848	0.423	0.031
G-12	Acryl	26.5	13.5	35	1.84	4.26	1.01	R	12.79	0.71	1.42	2.68	0.89	187.9	31.3	5.1	151.5	4.31	0.882	0.440	
G-13	Acryl	22.5	15.0	50	14.43	4.25	1.03	R	14.72	0.40	1.24	2.79	0.25	183.7	36.5	3.6	143.6	3.48	0.856	0.355	0.014
G-14	Acryl	22.5	13.5	35	14.43	4.25	1.03	R	13.23	0.39	1.23	2.78	0.10	164.1	33.2	4.1	126.8	3.44	0.847	0.351	0.006
G-15	Acryl	22.5	15.0	50	5.77	4.22	0.94	R	14.62	0.36	1.24	2.79	0.34	182.1	36.9	2.7	142.5	3.46	0.853	0.353	0.010
G-16	Acryl	22.5	13.5	35	5.77	4.22	0.94	R	13.19	0.34	1.23	2.78	0.27	163.1	30.0	2.2	131.0	3.54	0.873	0.362	0.010
G-17	Acryl	22.5	15.0	50	1.84	4.26	1.01	R	14.12	0.88	1.24	2.79	1.08	182.3	25.1	5.7	151.6	3.75	0.923	0.382	0.015
G-18	Acryl	22.5	13.5	35	1.84	4.26	1.01	R	12.61	0.89	1.23	2.78	1.16	162.7	20.8	5.4	136.6	3.77	0.929	0.385	0.001
G-19	Acryl	30	15.0	50	6.11	12.22	0.63	R	14.86	0.14	1.58	2.58	0.17	232.3	62.7	1.1	168.4	4.37	0.773	0.446	0.008
G-20	Acryl	30	15.0	50	6.23	5.59	1.57	R	15.00	0.04	1.58	2.58	0.04	232.8	78.4	0.3	154.0	3.98	0.703	0.406	0.014
G-21	Acryl	30	15.0	50	6.25	2.29	1.17	R	15.00	0.01	1.58	2.58	0.00	232.4	83.3	0.1	149.1	3.85	0.681	0.393	0.018
G-22	Acryl	30	15.0	50	6.11	12.22	0.63	C	14.65	0.35	1.58	2.58	0.37	232.3	55.5	3.2	173.7	4.55	0.804	0.464	0.006
G-23	Acryl	30	15.0	50	6.23	5.59	1.57	C	14.89	0.11	1.58	2.58	0.12	232.2	68.9	1.1	162.2	4.21	0.744	0.430	0.006
G-24	Acryl	30	15.0	50	6.25	2.29	1.17	C	14.79	0.22	1.58	2.58	0.06	232.3	75.6	3.0	153.7	4.02	0.711	0.411	0.019
G-25	Wood	30	15.0	50	1.84	4.26	1.01	R	13.66	1.34	1.58	2.58	1.67	232.2	67.3	10.6	154.3	4.18	0.738	0.426	0.039
G-26	Wood	30	13.5	35	1.84	4.26	1.01	R	12.59	0.91	1.57	2.57	1.13	207.7	33.1	7.3	167.3	5.00	0.883	0.510	0.015
G-27	Wood	20	15.0	50	1.84	4.26	1.01	R	13.65	1.35	1.11	2.84	1.33	163.2	19.7	9.1	134.4	3.35	0.940	0.342	0.006
G-28	Wood	20	13.5	35	1.84	4.26	1.01	R	12.49	1.02	1.10	2.83	1.19	145.6	8.2	6.0	131.4	3.60	1.008	0.367	0.006

Table 2
Test conditions and results for FC-series for variable fines content (acrylic flume, $\theta=30^\circ$, Roundish grain, $H=1.58$ m, $L=2.58$ m) (variable parameters: Materials-A and -B, $F_c=0$–100%, $w_c=50\%$, 35%).

Test no.	Total mass (kg)	Water content (%)	D_{50} (mm)	U_c	U_c'	F_c (%)	M_D (kg)	M_R (kg)	$\sum(l_j m_j)$ (kg m)	Initial potent. energy E_P (J)	Kinetic energy E_k (J)	Residual potential energy E_{PR} (J)	Dissip. energy E_D (J)	e_D (J/m/kg)	$e_{DP}/(g \tan\theta)$	Friction coeff. μ	Max. dev. of μ divided by av. of μ
FC-1	15	50	1.24	12.2	0.61	0	14.22	0.78	1.27	232.3	72.1	4.5	155.6	4.10	0.725	0.418	
FC-2	15	50	1.12	15.5	0.66	5	14.10	0.90	0.67	232.3	57.8	10.0	164.5	4.44	0.785	0.453	0.021
FC-3	15	50	0.99	22.5	0.78	10	13.85	1.15	1.62	232.3	50.2	7.9	174.2	4.66	0.824	0.476	0.032
FC-4	15	50	0.85	29.1	0.74	15	13.35	1.65	2.11	232.3	44.9	12.6	174.7	4.78	0.844	0.488	0.023
FC-5	15	50	0.77	41.8	0.89	20	14.80	0.20	0.28	232.3	62.9	1.4	167.9	4.37	0.772	0.446	0.011
FC-6	15	50	0.68	60.0	0.79	25	14.00	1.00	1.21	232.3	64.4	8.0	159.8	4.28	0.757	0.437	0.018
FC-7	15	50	0.58	72.8	0.28	30	14.75	0.25	0.33	232.3	87.2	1.8	143.3	3.73	0.660	0.381	0.019
FC-8	15	50	0.08	69.4	0.46	50	11.87	3.13	0.90	232.3	69.1	43.6	119.6	3.79	0.670	0.387	0.012
FC-9	15	50	0.05	14.8	1.46	100	12.79	2.21	1.02	232.3	70.7	28.4	133.2	3.92	0.692	0.400	0.001
FC-10	13.5	35	1.24	12.2	0.61	0	12.43	1.07	1.56	209.0	47.9	7.2	154.0	4.58	0.809	0.467	0.037
FC-11	13.5	35	1.12	15.5	0.66	5	12.20	1.30	1.90	209.0	33.0	8.8	167.3	5.01	0.886	0.511	0.036
FC-12	13.5	35	0.99	22.5	0.78	10	12.40	1.10	1.50	209.0	28.0	8.0	173.0	5.17	0.913	0.527	0.010
FC-13	15	50	2.00	20.2	0.74	0	13.55	1.45	1.72	232.3	77.4	12.1	142.8	3.89	0.688	0.397	0.005
FC-14	15	50	1.86	24.5	0.78	5	12.75	2.25	3.10	232.3	70.5	16.1	145.7	4.04	0.715	0.413	0.023
FC-15	15	50	1.71	42.4	1.09	10	14.25	0.75	0.83	232.3	69.0	6.2	157.0	4.18	0.738	0.426	0.019
FC-16	15	50	1.55	81.6	1.59	15	13.65	1.35	1.46	232.3	56.1	12.0	164.2	4.48	0.791	0.457	0.039
FC-17	15	50	1.39	101.0	1.40	20	13.95	1.05	1.33	232.3	88.5	8.2	135.6	3.63	0.642	0.371	0.012
FC-18	15	50	1.12	153.9	0.87	25	14.21	0.80	0.85	232.3	85.9	7.2	139.3	3.71	0.656	0.379	0.013
FC-19	15	50	0.90	206.4	0.35	30	14.60	0.21	0.31	229.2	82.1	4.4	142.7	3.76	0.664	0.384	0.070
FC-20	15	50	0.08	41.7	1.02	50	11.32	3.68	2.83	232.3	73.6	42.0	116.6	3.65	0.645	0.372	0.031

expressed as

$$\mu = e_D/g = R_d \tan\theta \tag{11}$$

Test results and energy calculations

In a series of tests (Hiraga, 2008), test conditions were changed parametrically as listed in Tables 1 and 2. In G-series (from G-1 to G-28) of Table 1, mean grain size (D_{50}=1.84–14.4 mm), grain shape (roundish or angular), flume angle (θ=20–30°) were parametrically varied using the acrylic or wooden flume. The value of water content was chosen as w_c=35% or 50% in this test, which corresponds to the density, 1.8 t/m^3 or 1.67 t/m^3 assuming the average solid density as 2.5 t/m^3 and the water saturation in actual debris flows. In FC-series (from FC-1 to FC-20) of Table 2, the fines content F_c (weight percentage of fines, grain size $<$0.075 mm) of two granular materials (A and B) was changed stepwise from 0% to 100% mainly for w_c=50%, using the acrylic flume of θ=30°. Tables 1 and 2 show pertinent test conditions, calculated energies and the equivalent friction coefficients μ for all the tests.

In most case, the same test was repeated twice under the same conditions to know its reproducibility in the test result. The deviation of the equivalent friction coefficient μ defined as $(\mu_{max}-\mu_{mean})/\mu_{mean}$, ($\mu_{max}$=the maximum or larger value in the repeated tests, μ_{mean}=the mean value) is listed for each test at the last column in the tables, while the blank line there indicates that the test was done only once in that particular case. The deviation of μ shown in Tables 1 and 2 is mostly less than a few percent though the maximum value is 7%, indicating that the repeatability in measuring the energy and the friction coefficient is generally well despite apparent difficulty in repeating the test in exactly the same way in every detail.

Effects of grain size curves and grain shape

Three soil samples with parallel grain size curves on the semi-log chart in Fig. 5 were used to examine the effect of mean grain size D_{50} in the acrylic flume with the angle θ=30°. Fig. 6(a) exemplifies the time histories of the flow velocity at the outlet of the flume measured by the digital image sensor and calculated by Eq. (4). The velocity is extremely variable with time, starting with high velocity for less than a second, followed by much lower velocity for a few seconds with intermissions of no flow in between. The mass discharge for the same test shown in Fig. 6(b) measured by the electronic balance is spiky reflecting the inertia of large gravels dropping on the balance. In order to eliminate the spikes, the signal is approximated by a curve of an exponential function, which indicates that primary mass discharge occurred in the first one second despite sustained flow in the later time. Two test results under the same condition shown in Fig. 6(a) and (b) are almost coincidental, indicating good repeatability in this case.

In Fig. 7(a) and (b), time histories of flow velocity and mass discharge, respectively, which were obtained from tests repeated twice for w_c=35% and the flume angle

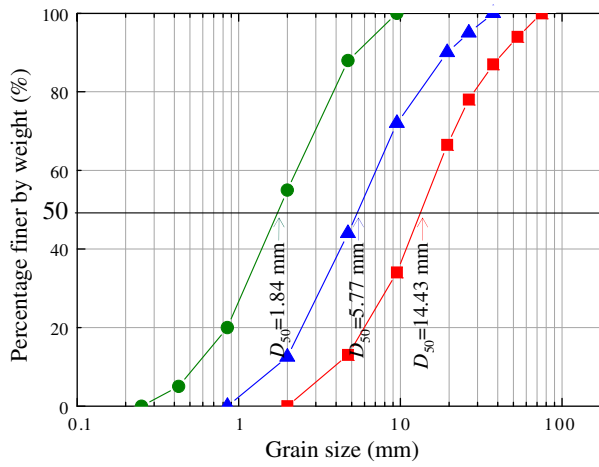

Fig. 5. Grain size curves of granular materials with different D_{50}.

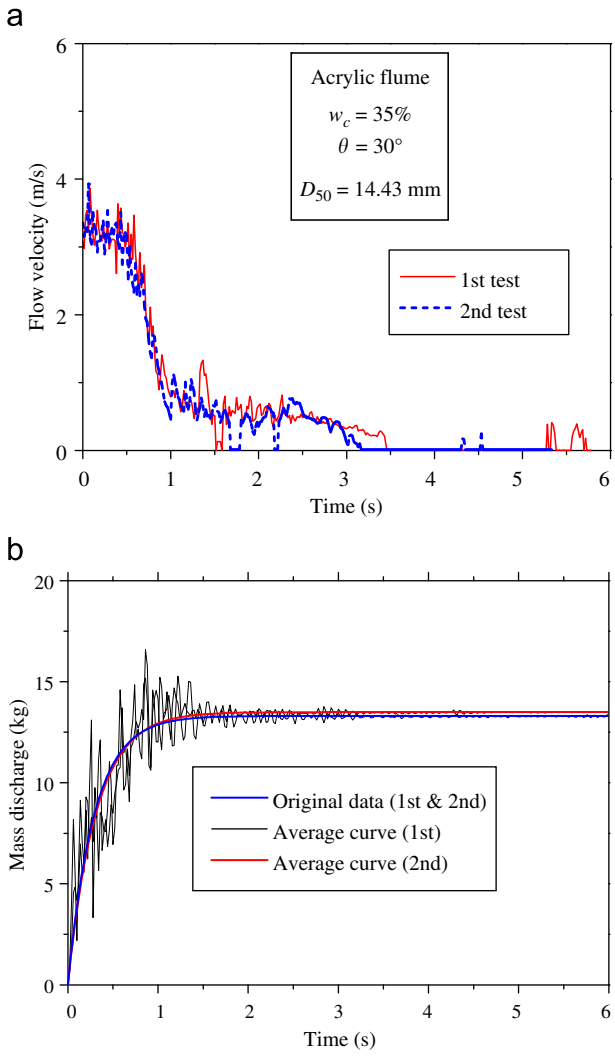

Fig. 6. Time histories of flow velocity at the outlet of flume measured by digital image sensor (a) and mass discharge measured by electronic balance (b) (Test G-2).

$\theta=30^\circ$ are shown for the materials of $D_{50}=14.43$, 5.77 and 1.84 mm. The larger the D_{50}-value, the faster the flow velocity and mass discharge, though the difference is not so significant. Fig. 7 shows that the granular flow is obviously transient; its velocity and discharge rate greatly change with time. In the following data reductions, however, the cumulative energies as a batch test are considered as a whole. Namely, the kinetic energy at the flume outlet E_K summed up during the test in Eq. (2) and the residual potential energy of soils in the flume at the end of the test E_{PR} calculated in Eq. (5) are subtracted from the initial potential energy E_{PI} in Eq. (6) to quantify the cumulative dissipated energy E_D during the batch test as in Eq.(1). The dissipated energy ratio $R_d=(e_{DP}/g\tan\theta)$ in Eq.(10) and the equivalent friction coefficient $\mu=R_d\tan\theta$ in Eq.(11) for tests of the flume angle $\theta=30^\circ$ are tabulated in Table 1 (from G-1 to G-6). Similarly, R_d and μ are calculated for the corresponding test results for $\theta=26.5^\circ$ and 22.5° and listed in Table 1 (from G-7 to G-18).

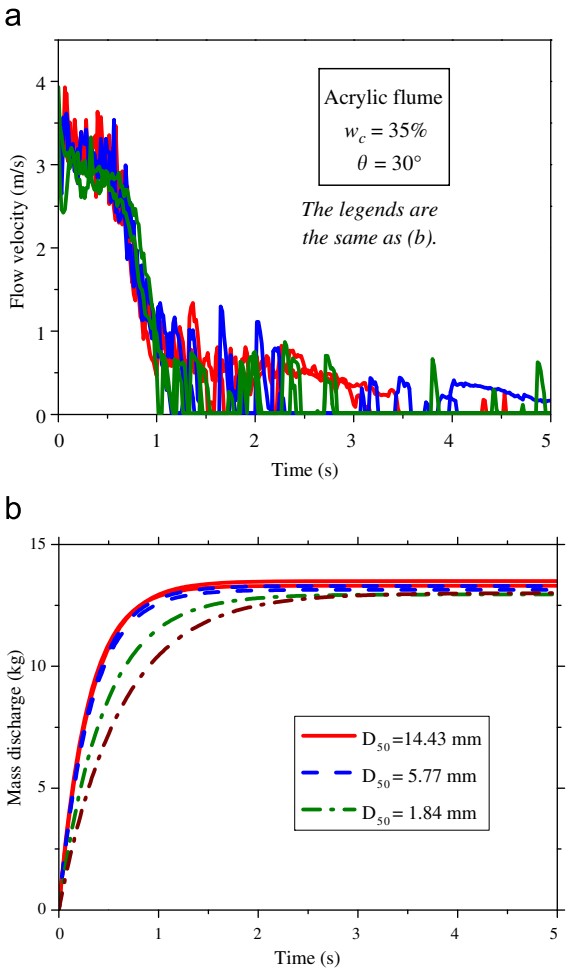

Fig. 7. Time histories of flow velocity (a) and mass discharge (b) for the mean grain size $D_{50}=14.43$, 5.77, 1.84 mm.

All these values are plotted versus the mean grain size D_{50} in Fig. 8. Both R_d and μ tend to decrease gently with increasing D_{50}, indicating that granular flow of smaller particle size tends to dissipate more energy for all the water contents and flume angles tested here. The difference is 12% maximum between $D_{50}=1.84$ mm and 14.43 mm.

Then, soils with grain size curves illustrated in Fig. 9 of almost the same D_{50} but different uniformity coefficients were tested in the acrylic flume under the condition of $w_c=50\%$ and $\theta=30^\circ$. Not only fluvial soils of roundish particles but also artificially crushed stones of angular particles with exactly the same grain size curves were tested to compare the results. The values R_d and μ are listed at G-19–G-24 in Table 1 and also plotted versus U_c in Fig. 10. It can be seen from the figure that the dissipated energy becomes 14% larger with increasing U_c from 2.29 to 12.22, and also that the particle angularity tends to increase the energy dissipation by only 4–6%.

Effects of flume angle and water content

The flume angle was parametrically changed to investigate its effect on the energy dissipation in the granular flow. For the acrylic flume, 3 flume angles ($\theta=22.5^\circ$, 26.5°,

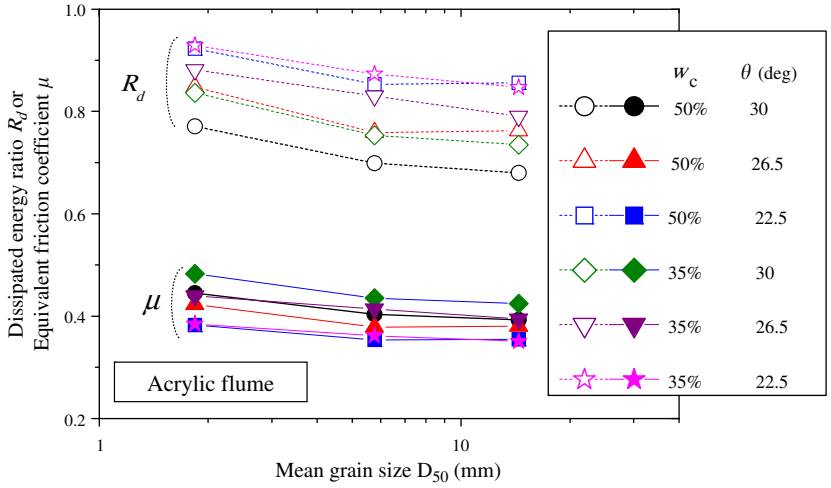

Fig. 8. Effect of mean grain size D_{50} on dissipated energy ratio R_d and equivalent friction coefficient μ for variable w_c and θ.

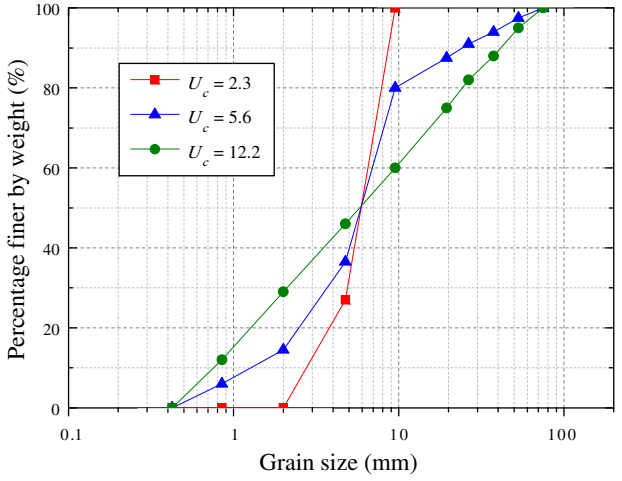

Fig. 9. Grain size curves of granular materials with different U_c.

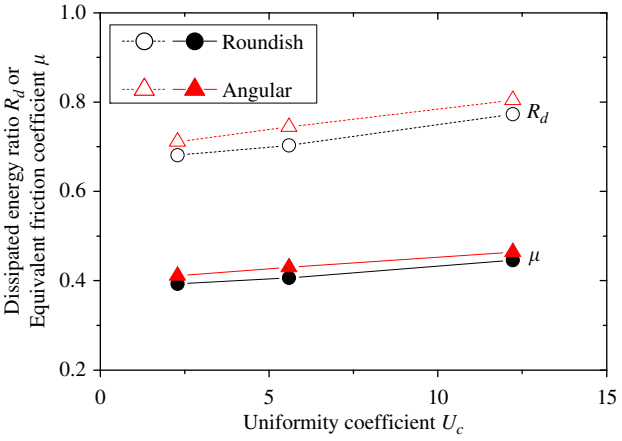

Fig. 10. Effect of uniformity coefficient U_c on dissipated energy ratio R_d and equivalent friction coefficient μ for roundish and angular particles.

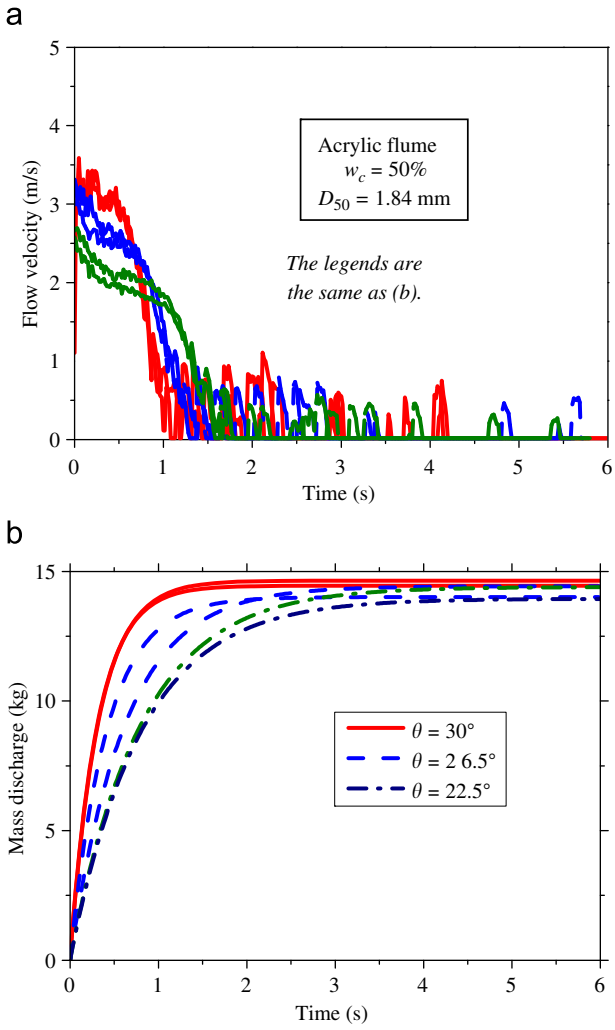

Fig. 11. Time histories of flow velocity (a) and mass discharge (b) for slope angle θ=30°, 26.5°, 22.5°.

30°) were chosen for 3 soil materials shown in Fig. 5 with the water content w_c=35%, 50%, whereas, for the wooden flume, 2 flume angles (θ=20°, 30°) for the soil of D_{50}=1.84 mm with w_c=35%, 50%. Fig. 11(a) and (b) depicts time histories of flow velocity for the tests using the acrylic flume and the soil of D_{50}=1.84 mm. Quite reasonably, the flow velocity and mass discharge become faster as the flume angle gets higher from θ=22.5° to 30°. The R_d and μ-values calculated from the test results are listed at G-1 to G-18 for the acrylic fume and at G-25 to G-28 for the wooden flume in Table 1 and also plotted versus θ in Fig. 12. It is observed that the dissipated energy ratio $R_d = e_D/g\tan\theta$ tends to decrease with increasing θ regardless of D_{50} and w_c both for the acrylic and wooden flumes. In contrast, the friction coefficient $\mu = e_D/g$ tends to increase with increasing flume angle θ. Two horizontal lines in the diagram represent the skin frictions already mentioned, indicating that the wooden flume has a little higher value than the acrylic flume. It is obvious that the μ-values tend to be either lower or higher than the μ_{skin}-values due to changing geotechnical parameters even under the same flume angle. The absolute value of friction coefficient is higher in the wooden flume, than in the acrylic flume if the results for the same water content is compared, presumably reflecting the difference in the measured μ_{skin}, though the μ_{skin}-values may not exactly represent skin frictions actually exerted during the flume test due to differences in water content and other conditions.

Effect of fines content

For test series FC1–FC20 in Table 2, two granular materials with different grain size distributions (D_{50}=1.24, U_c=12.2, C_c=0.61 and D_{50}=2.00, U_c=20.2, C_c=0.74) were prepared by mixing sands and gravels (C_c stands for the coefficient of curvature). Then, non-plastic fines made from rock flour finer than 0.075 mm in grain size were added stepwise to each of them from F_c=0% to 100% to make two types of materials of different fines content F_c (named here Materials-A and -B) as illustrated in Fig. 13. They were used to examine the effect of F_c in the acrylic

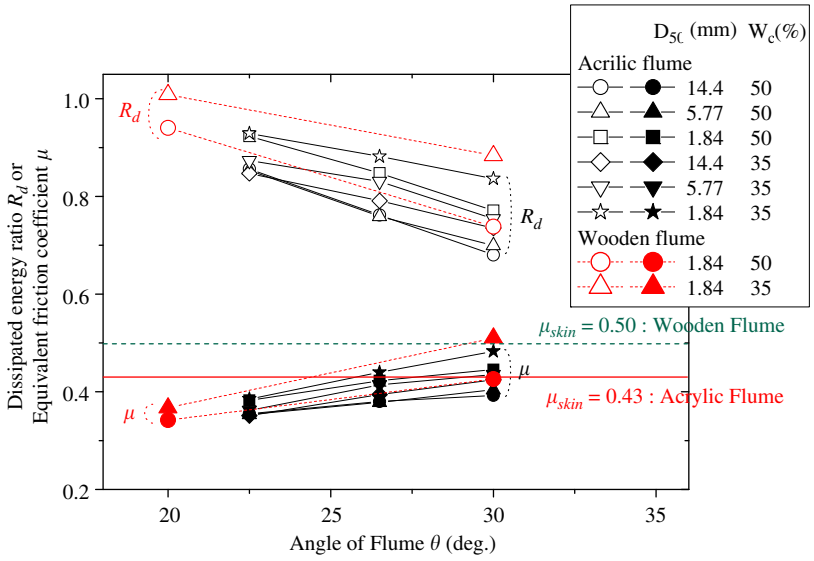

Fig. 12. Effect of flume angle θ on dissipated energy ratio R_d and equivalent friction coefficient μ for acrylic and wooden flumes.

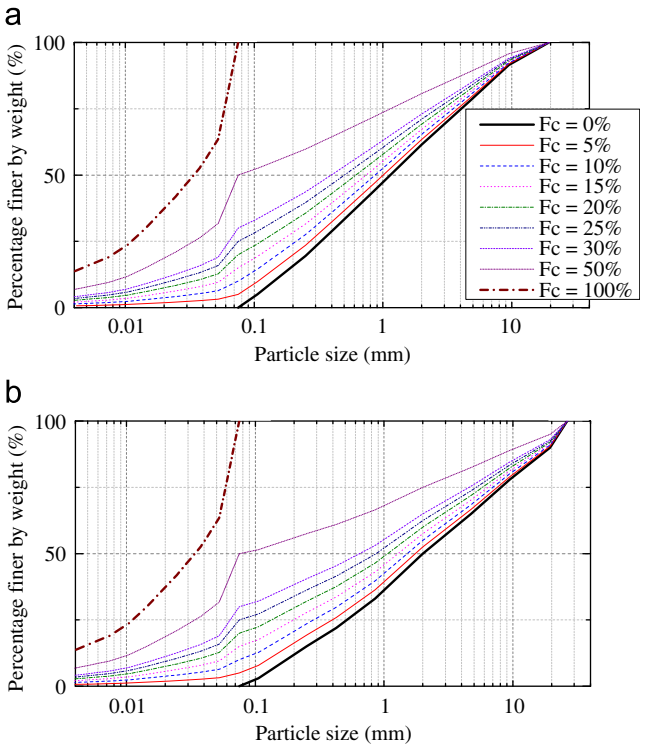

Fig. 13. Grain size curves of granular materials, A and B, with parametrically varying F_c. (a) A-grading and (b) B-grading.

flume of $\theta=30^\circ$. In Fig. 14(a) and (b), time histories of flow velocity and mass discharge are shown for Material-A of $F_c=0$, 15, 30, 100% and $w_c=50\%$. Though there are some differences between the repeated tests of the same conditions, the trend is obvious that higher velocity sustains longer and mass discharge occurs faster for $F_c=30\%$ in particular and that the mass discharge rate is much slower for $F_c=15\%$ than other F_c-values.

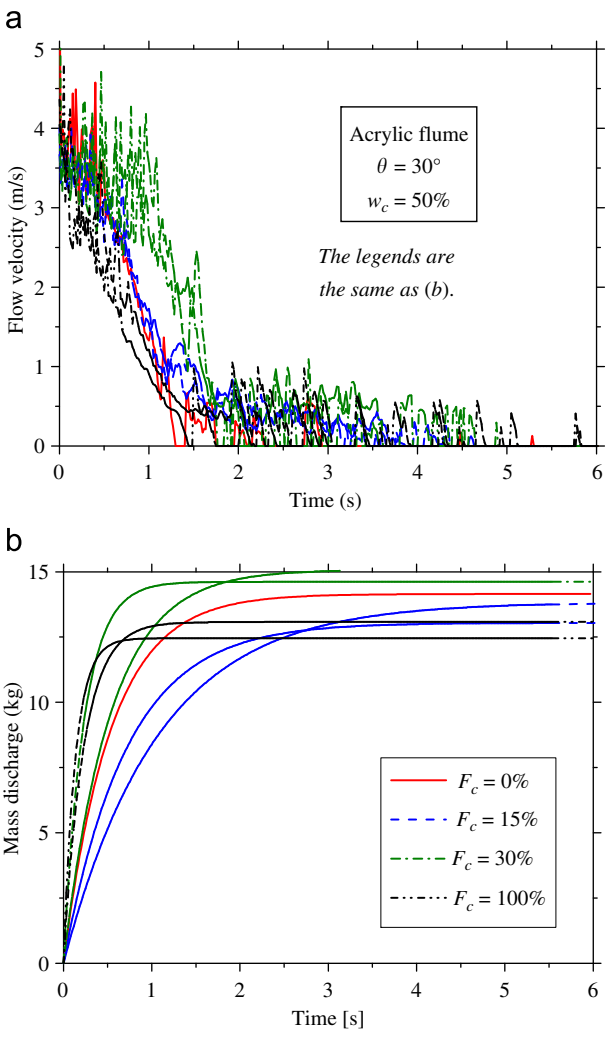

Fig. 14. Time histories of flow velocity (a) and mass discharge (b) for fines content F_c=0%, 15%, 30%, 100%.

From all the test results of FC-series using Materials-A and -B, dissipated energy ratio $R_d = e_{DP}/g\tan\theta$ and the equivalent friction coefficient $\mu = R_d\tan\theta$ are calculated and tabulated in Table 2 (from FC-1 to FC-20). All these values are plotted versus fines content F_c in Fig. 15. Both R_d and μ first increase until $F_c \fallingdotseq 15\%$ (both for $w_c = 50\%$ and 35%), then show sudden downturn to the lowest values at $F_c \fallingdotseq 20$–30%, which is followed by an almost constant low value up to $F_c = 100\%$. The trends are almost identical for Materials-A and -B, though the changes in B are slightly lagged compared to A presumably due to the difference in the grain size curves.

Superposed on the same diagram are the extents of critical fines content CF_c (12.6–15.4% for A and 11.1–14.4% for B) evaluated from the theoretical equation (Kokusho, 2007)

$$CF_c = (n_c - n_c n_f)/(1 - n_c n_f) \tag{12}$$

here, the porosity of coarse soil (sand and gravel) n_c and that of fine soil n_f are calculated from $n_c = (\rho_{s_c} - \rho_{d_c})/\rho_{s_c}$ and $n_f = (\rho_{s_f} - \rho_{d_f})/\rho_{s_f}$, respectively, where ρ_{s_c}, ρ_{sf}=solid densities for coarse and fine soil particles and ρ_{d_c}, ρ_{df}=soil dry densities for coarse and fine soils. The values of the soil particle density; ρ_{s_c}, ρ_{s_f}, minimum and maximum dry densities; $\rho_{d_{min}}$, $\rho_{d_{max}}$ which were obtained using the standardized test method for gravelly soils (the Japanese Industrial Standard JIS 1224: 2009), and the extents of values in n_c, n_f corresponding to the minimum and maximum dry densities are listed in Table 3 for Materials-A and -B. The extents of CF_c calculated from Eq. (12) for the two materials are also listed in the table assuming that the maximum or minimum density occurs at the same time in the coarse and fine soils.

The critical fines content CF_c is an index often used in granular mechanics which corresponds to the state where fine particles saturate the void of coarser grains and start to overflow, changing the soil fabric from grain-supporting to matrix supporting. Because the peaks for R_d and μ occur within the extent of CF_c-values both for Materials-A and -B as observed in the figure, the soil fabric change seems to

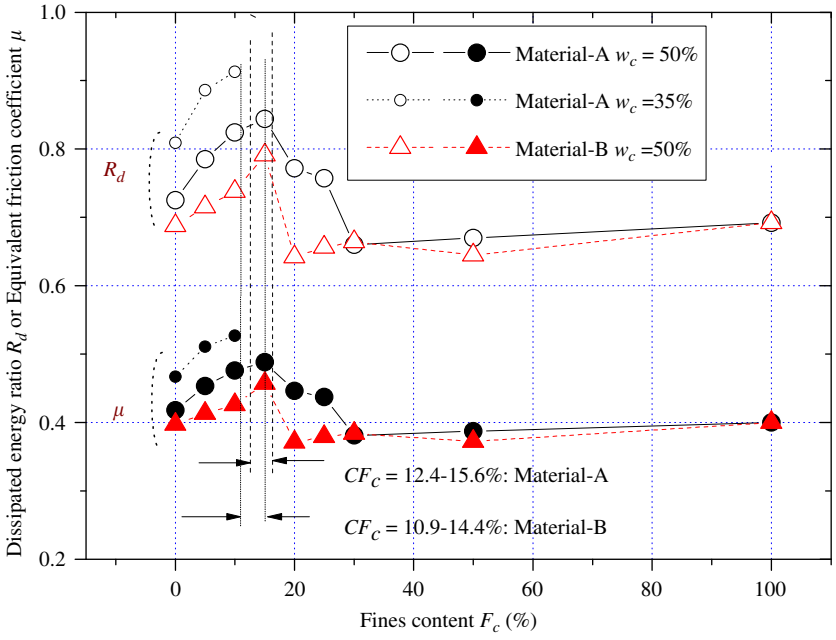

Fig. 15. Effect of fines content F_c on dissipated energy ratio R_d and equivalent friction coefficient μ for 2 granular materials, A and B, tested in the acrylic flume.

Table 3
Critical fines contents CF_c and related values for Materials-A and -B.

Soil material		Soild density ρ_s (g/cm^3)	Min. soil density ρ_{dmin} (g/cm^3)	Max. soil density ρ_{dmax} (g/cm^3)	Extent of values corresponding to min.–max. soil density		
					Porosity of sand and gravel n_c	Porosity of fines n_f	CF_c
Material-A	Sand and gravel	2.65	1.68	2.11	0.366–0.204	–	0.156–0.126
	Fines	2.74	0.88	1.54	–	0.679–0.438	
Material-B	Sand and gravel	2.70	1.74	2.21	0.344–0.181	–	0.144–0.110
	Fines	2.74	0.88	1.54	–	0.679–0.438	

dramatically decrease the dissipated energy and the associated friction coefficient, facilitating a transition from granular flow to high speed mud flow. It may well be inferred qualitatively that a similar mechanism may also be involved in actual debris flow.

Discussions

All the friction coefficients obtained by the flume tests listed in Tables 1 and 2 are plotted again versus the flume gradient β with different symbols on the same diagram in Fig. 16. The plots are all on or below the diagonal line $\mu=\beta$ quite logically because otherwise the flow could not occur. The μ-values tend to increase slightly with increasing slope gradient β in the both flumes at almost the same rate as already indicated in Fig. 12, too.

Equivalent friction coefficients were quantified in situ previously from debris flows induced by rains and earthquakes, which were found to be dependent on various parameters. Among the parameters, it is known that the greater the debris volume, the friction coefficient tends to be smaller (e.g. Hsu, 1975). The same trend has also been found in case studies of a number of slope failures during the 2004 Niigataken Chuetsu earthquake by Kokusho et al. (2009).

In this test series, in which the effect of slope gradient was focused rather than the debris volume, the increasing trend of friction coefficient with slope gradient has been clearly observed both in acrylic and wooden flumes as shown in Fig. 16. However, the increasing rate seems moderate compared to the $\mu=\beta$ line. Since the skin friction does not seem to change with slope angle, inter-particle movements inside the flow may increase the equivalent friction coefficient with increasing slope gradient. Much more research is certainly needed to know exactly how the energy dissipation inside the granular flow changes due to changing slope gradient.

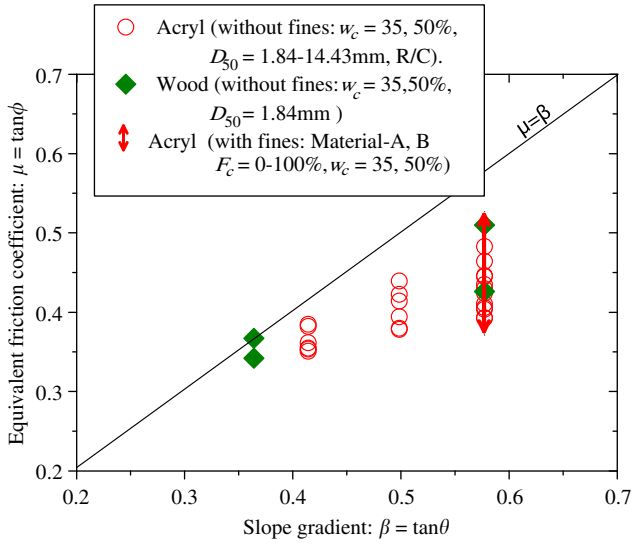

Fig. 16. Equivalent friction coefficient $\mu=\tan\varphi$ plotted versus flume gradient $\beta=\tan\theta$ for all test results with different materials and test conditions.

Conclusions

A series of flume tests were conducted for soil samples with different geotechnical parameters to study energy dissipation mechanisms in granular flow from the granular mechanics point of view, yielding the following major findings:

(1) With decreasing mean grain size D_{50}, the dissipated energy ratio R_d and the equivalent friction coefficient μ tend to increase for water contents and slope angles tested in the acrylic flume, though their increments are not so large (12% maximum between $D_{50}=14.43$ and 1.84 mm). The R_d and μ-values tend to increase with increasing uniformity coefficient U_c (14% between $U_c=2.29$ and 12.22). Particle angularity tends to increase the energy dissipation only 4–6% if fluvial gravels and artificial crushed stones are compared.
(2) The dissipated energy ratio R_d tends to decrease with increasing θ regardless of D_{50} and w_c both for the acrylic and wooden flumes, while the friction coefficient μ tends to increase with increasing θ. The absolute value of friction coefficient is higher in the wooden flume than in the acrylic flume, presumably reflecting the difference in the measured skin friction.
(3) According to the tests using two materials with slightly different grain size curves, both R_d and μ tend to increase to peak values with increasing fines content F_c up to $F_c=15\%$, then suddenly turn down to the lowest values at $F_c=20$–30%, followed by almost constant low values up to $F_c=100\%$.
(4) This value of F_c corresponding to the peak almost coincides with critical fines content CF_c of sand–gravel mixture at which fines saturate the voids of sands and gravels and start to overflow, changing the soil fabric from grain-supporting to matrix-supporting.
(5) This may indicate that the granular flow may change to mud flow with lower equivalent friction coefficient near CF_c. Thus, the effect of fines content F_c of non-plastic fines seems important because it may potentially change the flow type from slow-speed granular flow to high speed mud flow with a slight change in F_c.
(6) It is shown in this test series that the measured friction coefficients tend to increase moderately with increasing slope gradient both in acrylic and wooden flumes. Since the skin friction does not seem to change with slope angle, increasing inter-particle movements with increasing slope gradient seem to be responsible for this.

Acknowledgments

A part of this research was supported by Special Coordination Funds for Promoting Science and Technology,

"Earthquake damage in active-folding areas—creation of a comprehensive data archive and suggestions for its application to remedial measures for civil-infrastructure systems" of Japan Science and Technology Agency. Graduate and under-graduate students, who contributed to this laborious laboratory experiments between 2005 and 2010 in Civil Engineering Department of Chuo University are gratefully acknowledged.

References

Hiraga, Y., 2008. Evaluation of Dissipated Energy in Debris Flow for Granular Materials in Flume Test. M.S. Thesis. Graduate School of Chuo University.

Hsu, J., 1975. Catastrophic debris streams generated by rockfalls. Geological Society of America Bulletin 86 (50117), 129–140.

Japanese Geotechnical Society, 2003. Debris Flow. Geotechnical Note 12. JGS.

Kokusho, T., 2005. Extreme events in geohazards in Asia. In: Proceedings of the International Conference on Geotechnical Engineering for Disaster Mitigation and Rehabilitation. Singapore, pp. 1–20.

Kokusho, T., 2007. Liquefaction strengths of poorly-graded and well-graded granular soils investigated by lab tests. In: Proceedings of the Fourth International Conference on Earthquake Geotechnical Engineering. Thessaloniki, Springer, pp. 159–184.

Kokusho, T., Ishizawa, T., Nishida, K., 2009. Travel distance of failed slopes during 2004 Chuetsu earthquake and its evaluation in terms of energy. Soil Dynamics and Earthquake Engineering 29, 1159–1169 (Elsevier).

Takahashi, T., 1980. Debris flow on prismatic open channel. Proceedings of the American Society of Civil Engineers 106 (HY3), 381–396.

Yasuda, M., Endo, N., Sunamura, T., 2008. Laboratory experiments of debris flows triggered by spontaneous failure of a sediment pile: a scaling law of the friction coefficient considering water content and flow mass. Transactions, Japanese Geomorphological Union 29 (2).